High-Performance Large Air-Gap Capacitive Wireless Power Transfer System for Electric Vehicle Charging

Brandon Regensburger, Ashish Kumar, Sreyam Sinha, Kate Doubleday, Saad Pervaiz,
Zoya Popovic and Khurram Afridi
Department of Electrical, Computer, and Energy Engineering
University of Colorado Boulder
Boulder, USA

***Abstract*— This paper introduces a high-performance large air-gap capacitive wireless power transfer (WPT) module as part of a multi-modular capacitive WPT system for electric vehicle charging. This WPT module utilizes two pairs of metal plates separated by an air-gap as the capacitive coupler, incorporates L-section matching networks to provide gain and reactive compensation, and is driven by a GaN-based inverter operating at 6.78 MHz. The system achieves high efficiency and simplicity by eliminating the need for high-voltage capacitors, and instead utilizes the parasitic capacitances formed between the coupling plates and the vehicle chassis and roadway as part of the matching networks. This paper also presents a comprehensive design methodology for the capacitive WPT system that guarantees high performance by ensuring zero-voltage switching of the inverter transistors, and by selecting matching network component values to maximize efficiency under practical constraints on inductor quality factor and self-resonant frequency. Two prototype 6.78-MHz 12-cm air-gap capacitive WPT systems have been designed, built and tested. The first prototype with 625 cm^2 coupling plate area transfers up to 193 W of power and achieves an efficiency greater than 90%, with a power transfer density of 3 kW/m^2. The second prototype with 300 cm^2 coupling plate area transfers up to 557 W of power and achieves an efficiency of 82%, with a power transfer density of 18.5 kW/m^2, which exceeds the state-of-the-art for capacitive WPT systems by more than a factor of four.**

***Keywords*—capacitive wireless power transfer; large air-gap; wireless power transfer; electric vehicle; high efficiency; high power transfer density; matching networks; high frequency.**

I. INTRODUCTION

Most wireless power transfer (WPT) systems for electric vehicle (EV) charging rely on inductively coupled coils to transfer power across large air-gaps. Inductive WPT systems often require ferrites that are expensive and incur high core losses, limiting their frequency of operation [1]. On the other hand, capacitive WPT systems transmit power across air-gaps using electric fields between conductive plates. Capacitive WPT systems do not require ferrites, enabling high operating frequencies with smaller components. Large air-gap capacitive WPT systems suitable for EV charging have recently been explored in [2]-[11]. A multi-modular large air-gap capacitive WPT architecture was introduced in [2], which utilizes phased-array field focusing to cancel fringing electric fields in accordance with safety regulations [12]. Design guidelines for a single module of this multi-modular architecture were presented in [6] and [8]. This paper builds upon the work in [6] and [8] to design and demonstrate a high-performance large air-gap capacitive WPT system for EV charging, suitable as one module of the multi-modular architecture of [2]. Two prototype 6.78-MHz 12-cm air-gap capacitive WPT systems have been designed, built and tested. The first prototype with 625 cm^2 coupling plate area transfers up to 193 W of power and achieves an efficiency greater than 90%, with a power transfer density of 3 kW/m^2. The second prototype with 300 cm^2 coupling plate area transfers up to 557 W of power and achieves an efficiency of 82%. The 18.5 kW/m^2 power transfer density of this prototype system exceeds the state-of-the-art for capacitive WPT systems by more than a factor of four.

The remainder of this paper is organized as follows. Section II presents the architecture and operating principle of the capacitive WPT system. Section III introduces a design and optimization methodology for the capacitive WPT system. Section IV presents experimental results for two prototype capacitive WPT systems. Finally, Section V summarizes and concludes the paper.

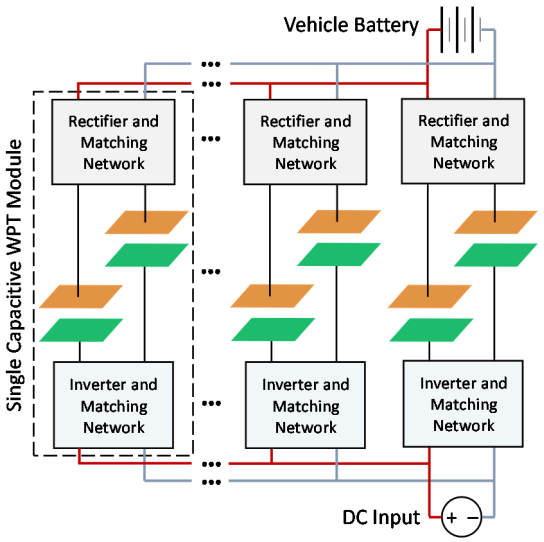

Fig. 1. Architecture of a multi-modular large air-gap capacitive WPT system suitable for EV charging applications. Each module comprises two pairs of coupling plates, a high-frequency inverter and rectifier, and matching networks that provide voltage or current gain and reactive compensation.

This work was supported by the Advanced Research Projects Agency – Energy (ARPA-E), Department of Energy under Award Number DE-AR0000618.

II. Capacitive WPT System Archetecture

The architecture of a multi-modular capacitive WPT system for EV charging is shown in Fig. 1 [2], [5]. Wireless power transfer in each module of this system is achieved using two pairs of conducting plates, one pair embedded in the road, and the other in the vehicle bottom, separated by a large air-gap. An inverter converts the dc input voltage into high-frequency ac, which is fed into a resonant matching network that steps up the voltage. This creates a high voltage at the road side of the coupling plates, enabling high power transfer with low displacement currents, and hence relatively low fringing fields. This network also partially compensates for the capacitive reactance of the coupling plates. On the vehicle side of the coupling plates is a second resonant matching network that steps the current back up (and the voltage down) to the level required to charge the EV battery. Furthermore, this network provides the remaining compensation for the plate reactance. Finally, a high-frequency rectifier interfaces the module to the EV battery.

III. System Design And Optimization

An example implementation of a single module of the multi-modular capacitive WPT architecture of Fig. 1 is shown in Fig. 2. It comprises a full-bridge inverter, L-section matching networks that provide the required gains and compensation, and a full-bridge rectifier. In this paper, the capacitive WPT system of Fig. 2 is evaluated in a realistic EV charging scenario, including the effects of the vehicle chassis and the road, as shown in Fig. 3(a). The vehicle chassis and the road can be modeled by metal sheets, as shown in Fig. 3(b). As can be seen from Fig. 3, parasitic capacitances are formed between the coupling plates and the vehicle chassis, as well as between the plates and the road. The system is designed to operate at the Industrial, Scientific and Medical (ISM) frequency of 6.78 MHz. At this high frequency, the parasitic capacitances can significantly impact the power transferred across the coupling plates, and hence must factor in the design of the system. In this work, these parasitic capacitances are incorporated into the main power transfer mechanism of the capacitive WPT module by utilizing them as the capacitors of the two L-section matching networks shown in Fig. 2. This has the additional advantage of eliminating discrete high-voltage capacitors from the inverter and rectifier PCBs, hence enhancing the efficiency and reliability of the system, and reducing its component cost. A capacitive WPT module with the L-section capacitors replaced by the parasitic capacitances is shown in Fig. 4(a). The capacitors labeled C_{pr} represent the parasitic capacitances between the coupling plates and the road, and those labeled C_{pv} represent the parasitic capacitances between the plates and the vehicle chassis. The nodes R and VC represent the road and the vehicle chassis, respectively. In order for the parasitic capacitances to be utilized as the matching network capacitors,

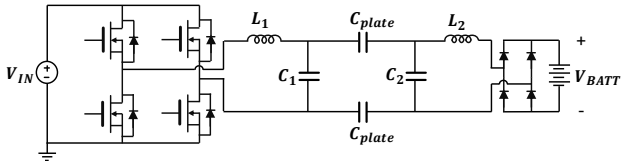

Fig. 2. Example implementation of a single module of the multi-modular capacitive WPT architecture of Fig. 1.

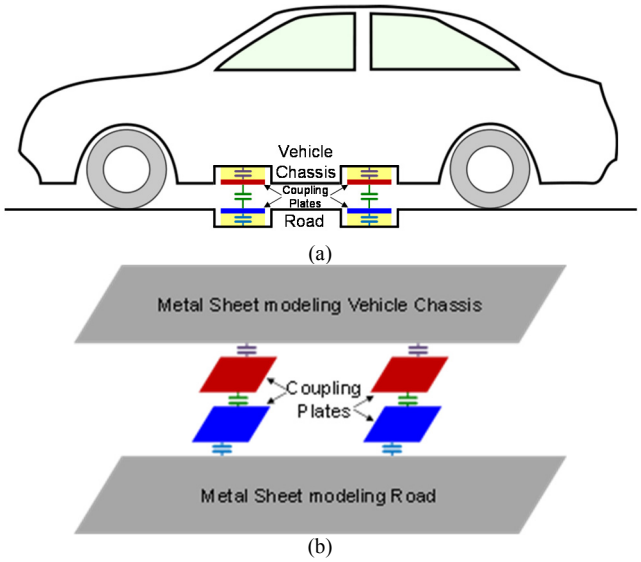

Fig. 3. The coupling and parasitic capacitances involved in a capacitive WPT system for EV charging: (a) physical origin, and (b) with metal sheets mimicking vehicle chassis and road.

the two parasitic capacitances on either side of the coupling plates must combine in series. This can be ensured by preventing parasitic ground currents (shown as I_{gr} and I_{gv} in Fig. 4(a)) from flowing through the impedances between the road/chassis and the inverter/rectifier ground (shown as Z_{gr} and Z_{gv} in Fig. 4(a)). To accomplish this, the inductors of the matching networks are split into two equal halves, with one half placed in the forward path, and the other in the return path, as shown in Fig. 4(b). The forward and return paths of this circuit are symmetric, resulting in zero voltage at nodes R and VC, and hence zero parasitic ground currents. The series combination of

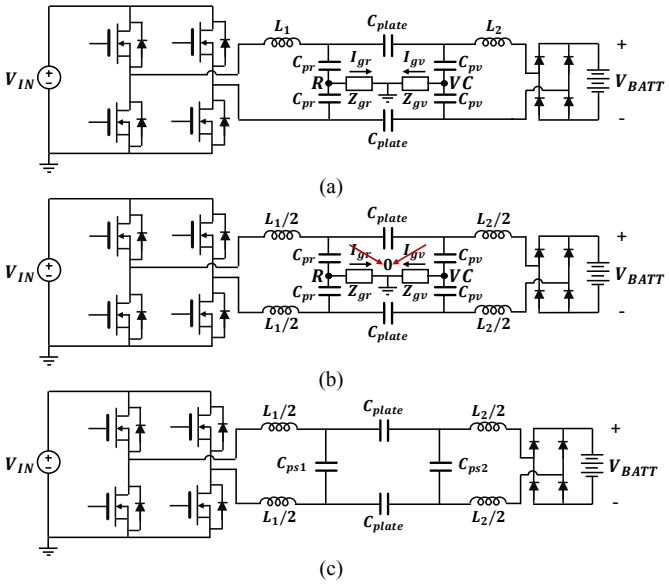

Fig. 4. Schematic of the capacitive WPT module utilizing L-section matching networks with: (a) the matching network capacitors replaced by the parasitic capacitances between the coupling plates and the vehicle chassis and roadway; (b) the matching network inductors symmetrically split in two, eliminating parasitic ground currents and enabling the parasitic capacitances to be combined in series; and (c) the matching network capacitors realized using the series combination of the parasitic capacitances.

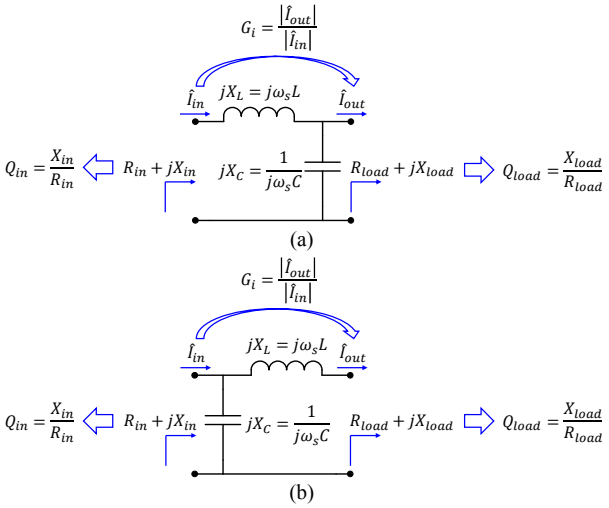

Fig. 5: Characterization of L-section matching networks that provide gain and compensation: (a) road-side network, and (b) vehicle-side network.

the parasitic capacitances can now be utilized as the matching network capacitors, as shown in Fig. 4(c).

The two L-section matching networks of Fig. 4(c) are designed to provide voltage or current gain, and to compensate for the capacitive reactance of the coupling plates. An analytical framework for designing L-section matching networks that provide both gain and compensation was introduced in [6], [13]. The work in [8] provides constraints on realizable inductance values for these matching networks, based on achievable inductor quality factors and self-resonant frequencies. This paper leverages the analytical framework of [6] and combines it with the practical guidelines of [8] to develop a systematic design methodology for determining the optimal inductance and capacitance values that maximize the matching network efficiency. Under the analytical framework described in [6], an L-section network is characterized by three quantities: its current gain G_i, defined as $G_i = \frac{|\hat{I}_{out}|}{|\hat{I}_{in}|}$, where $|\hat{I}_{out}|$ and $|\hat{I}_{in}|$ are the amplitudes of the output and input currents of the network, respectively; its load impedance characteristic Q_{load}, defined as $Q_{load} = \frac{X_{load}}{R_{load}}$, where X_{load} and R_{load} are the imaginary and real parts of the load impedance, respectively; and its input impedance characteristic Q_{in}, defined as $Q_{in} = \frac{X_{in}}{R_{in}}$, where X_{in} and R_{in} are the imaginary and real parts of the input impedance, respectively. These quantities are illustrated for the road-side and vehicle-side matching networks of the capacitive WPT system of Fig. 4(c) in Fig. 5(a) and Fig. 5(b), respectively. Note that since the road-side network provides a step-up in voltage, its current gain G_i is less than 1; similarly, for the vehicle-side network, G_i is greater than 1. Furthermore, the compensation provided by the two networks is captured by their impedance characteristics (Q_{in}'s and Q_{load}'s). Assuming that the losses in the matching networks of the capacitive WPT system of Fig. 4(c) are dominated by the losses in the inductors, the efficiency of the two networks can be well-approximated in terms of their current gains and impedance characteristics as [6], [13]:

$$\eta_r \approx 1 - \frac{\frac{1}{G_{i,r}}\sqrt{\left(1-G_{i,r}^2\right)+Q_{load,r}^2}+Q_{in,r}}{Q_L}, \quad (1a)$$

$$\eta_v \approx 1 - \frac{G_{i,v}\sqrt{\left(1-\frac{1}{G_{i,v}^2}\right)+Q_{in,v}^2}-Q_{load,v}}{Q_L}. \quad (1b)$$

Here, $G_{i,r}$ and $G_{i,v}$ are the current gains, $Q_{in,r}$ and $Q_{in,v}$ are the input impedance characteristics, and $Q_{load,r}$ and $Q_{load,v}$ are the load impedance characteristics of the road-side and vehicle-side matching networks, respectively, and Q_L is the unloaded quality factor of the inductors, given by: $Q_L = \frac{2\pi f_s L}{R_L}$, where f_s is the operating frequency of the system, L is the inductance and R_L is the ac resistance of the inductor, quantifying its winding and core losses at the operating frequency. Using (1a) and (1b), and assuming similar quality factors for the road-side and vehicle-side inductors, the overall efficiency of the two matching networks can be approximated as:

$$\eta_{tot} \approx 1 - \frac{\frac{1}{G_{i,r}}\sqrt{\left(1-G_{i,r}^2\right)+Q_{load,r}^2}+Q_{in,r}+G_{i,v}\sqrt{\left(1-\frac{1}{G_{i,v}^2}\right)+Q_{in,v}^2}-Q_{load,v}}{Q_L}. \quad (2)$$

The design methodology presented here attempts to maximize the overall matching network efficiency η_{tot} by optimally selecting the current gains and impedance characteristics of the two matching networks, while also ensuring that the inverter of the capacitive WPT system is sufficiently inductively loaded to achieve zero-voltage switching (ZVS) of the inverter transistors. To minimize circulating currents, only the minimum inductive loading required for ZVS is desired. To better understand this, consider Fig. 6, which illustrates the high-to-low transition of the switch-node voltage of the full-bridge inverter of the capacitive WPT system of Fig. 4(c). It can be seen from Fig. 6(b) that the switch-node current is positive during this transition, enabling the output capacitances of the transistors Q_2 and Q_3 to be discharged. The amount of charge required to fully discharge these output capacitances, and hence achieve ZVS, is given by:

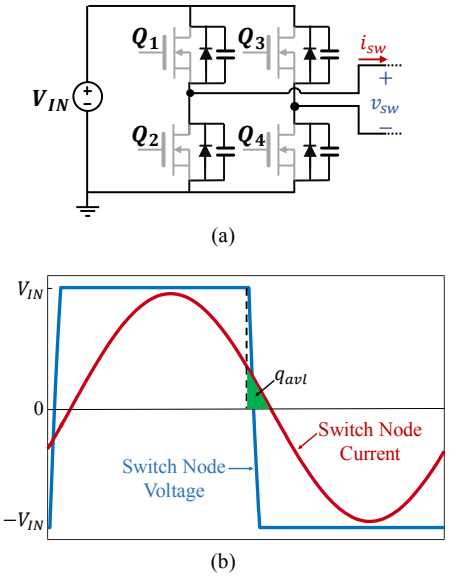

Fig. 6. High-to-low transition of the full-bridge inverter of the capacitive WPT system: (a) switch states during the transition, and (b) switch-node voltage and current demonstrating ZVS operation. The charge q_{avl} represents the maximum charge available in the switch-node current to discharge the output capacitances of the inverter transistors Q_2 and Q_3.

$$q_{ZVS} = 2C_{oss}V_{IN}. \quad (3)$$

Here, C_{oss} is the linear equivalent output capacitance of the inverter transistors, obtained using the transistor datasheet, and V_{IN} is the dc input voltage of the system. The ZVS-enabling charge given by (3) must be provided by the switch-node current. The maximum charge that the switch-node current can provide is illustrated in Fig. 6(b), and can be mathematically expressed as:

$$q_{avl} = \frac{I_{pk}}{2\pi f_s}(1 - \cos\phi). \quad (4)$$

Here, I_{pk} is the peak of the switch-node current, and ϕ is the phase lag of the switch-node current with respect to the switch-node voltage. To achieve ZVS with minimal circulating current, the available charge given by (4) must equal the charge required for ZVS given by (3). By relating the peak of the switch-node current I_{pk} to the input voltage V_{IN} and output power P_{OUT}, this results in the following constraint on the phase shift ϕ:

$$\phi = \cos^{-1}\frac{1}{1+\frac{8C_{oss}V_{IN}^2 f_s}{P_{OUT}}}. \quad (5)$$

The phase shift constraint of (5) corresponds to a constraint on the input impedance characteristic of the road-side matching network, $Q_{in,r}$, which can be expressed as:

$$Q_{in,r} = \frac{X_{in,r}}{R_{in,r}} = \tan\phi = \tan\left(\cos^{-1}\frac{1}{1+\frac{8C_{oss}V_{IN}^2 f_s}{P_{OUT}}}\right). \quad (6)$$

Using fundamental frequency analysis, the full-bridge rectifier of the capacitive WPT system of Fig. 4(c) can be modeled as an equivalent resistance, given by:

$$R_{rec} = R_{load,v} = \frac{8}{\pi^2}\frac{V_{BATT}^2}{P_{OUT}}. \quad (7)$$

Here, V_{BATT} is the voltage of the EV battery, and $R_{load,v}$ is the load resistance of the vehicle-side matching network, which is the same as the equivalent resistance presented by the rectifier R_{rec} (see Fig. 4(c)). Therefore, the load impedance of the vehicle-side matching network is purely resistive, resulting in the following design equation:

$$Q_{load,v} = \frac{X_{load,v}}{R_{load,v}} = 0. \quad (8)$$

An additional design constraint arises from the requirement that the voltage across the coupling plates must be limited to a value that prevents the fringing electric fields from exceeding safety limits [6]. This constraint can be expressed using the following relationships:

$$G_{i,r} = \frac{|\hat{I}_{plate}|}{|\hat{I}_{in,r}|} = \frac{2\pi f_s C_{plate}|\hat{V}_{plate}|}{\frac{\pi}{2}\frac{P_{OUT}}{V_{IN}\cos\phi}}, \quad (9a)$$

$$G_{i,v} = \frac{|\hat{I}_{out,v}|}{|\hat{I}_{plate}|} = \frac{\frac{\pi}{2}\frac{P_{OUT}}{V_{BATT}}}{2\pi f_s C_{plate}|\hat{V}_{plate}|}. \quad (9b)$$

Here, $\hat{I}_{plate}$ and $\hat{V}_{plate}$ are phasor representations of the safety-limited displacement current and voltage across the coupling plates, respectively, C_{plate} is the effective coupling capacitance (see Fig. 4), $\hat{I}_{in,r}$ is the input current of the road-side matching network expressed in phasor domain, and $\hat{I}_{out,v}$ is the output current of the vehicle-side matching network in phasor domain. Note that the phase shift ϕ in (9a) is computed using (5). Finally, the load impedance characteristic of the road-side network $Q_{load,r}$ is related to the input impedance characteristic of the vehicle-side network $Q_{in,r}$ by the coupling plate capacitance, and the current gain and load resistance of the vehicle-side network, as:

$$Q_{in,v} - Q_{load,r} = \frac{1}{\left(2\pi f_s\frac{C_{plate}}{2}\right)\left(G_{i,v}^2 R_{load,v}\right)}. \quad (10)$$

The proposed design methodology proceeds as follows: given the required output power P_{OUT}, EV battery voltage V_{BATT}, coupling capacitance C_{plate}, safety-limited coupling plate voltage $\hat{V}_{plate}$ and operating frequency f_s, the input impedance characteristic of the road-side network, the load impedance characteristic of the vehicle-side network, and the current gains of the two networks are determined using (6), (8) and (9), respectively. The load impedance characteristic of the road-side network, $Q_{load,r}$, is then swept iteratively over a wide range. For each value of $Q_{load,r}$, the corresponding value of the input impedance characteristic of the vehicle-side network $Q_{in,v}$ is computed using (10) and (7), and the required inductance and capacitance values of the two matching networks are obtained using the following expressions:

$$L_1 = \frac{\left(G_{i,r}\sqrt{\left(1-G_{i,r}^2\right)+Q_{load,r}^2} + G_{i,r}^2 Q_{in,r}\right)G_{i,v}^2 R_{load,v}}{2\pi f_s}. \quad (11a)$$

$$C_{ps1} = \frac{1-G_{i,r}^2}{2\pi f_s\left(G_{i,r}\sqrt{\left(1-G_{i,r}^2\right)+Q_{load,r}^2} - G_{i,r}^2 Q_{load,r}\right)G_{i,v}^2 R_{load,v}}. \quad (11b)$$

$$L_2 = \frac{\left(\sqrt{\left(G_{i,v}^2-1\right)+G_{i,v}^2 Q_{in,v}^2} - Q_{load,v}\right)R_{load,v}}{2\pi f_s}. \quad (12a)$$

$$C_{ps2} = \frac{1-\frac{1}{G_{i,v}^2}}{2\pi f_s\left(\sqrt{\left(G_{i,v}^2-1\right)+G_{i,v}^2 Q_{in,v}^2} + Q_{in,v}\right)R_{load,v}}. \quad (12b)$$

The inductors are then designed as single-layer air-core solenoids using the guidelines provided in [8]. Inductor designs that have quality factors below 250 and self-resonant frequencies below three times the operating frequency ($< 3f_s$) are discarded. For the remaining feasible designs, the overall matching network efficiency is computed using (2). This procedure identifies the most efficient feasible design of the matching networks of the capacitive WPT system of Fig. 4(c), and ensures ZVS of the inverter transistors with minimal circulating currents.

IV. Experimental Results

Two prototype 6.78-MHz 12-cm air-gap capacitive WPT systems designed using the procedure outlined in the previous section have been built and tested. The prototype systems are similar to the one shown in Fig. 4(c), with one difference being that the rectifier input is modeled and implemented as a resistor. A photograph of the first prototype capacitive WPT system is shown in Fig. 7. The coupling plates visible in Fig. 7(a) have dimensions of 17.68 cm × 17.68 cm, resulting in a total coupling plate area of 625 cm^2. The plates are implemented using 1 oz. copper pour in a printed circuit board (PCB). The

TABLE I. Component Values Used in the Two Prototype Capacitive WPT Systems

	C_{plate} [pF]	L_1 [μH]	L_2 [μH]	C_{ps1} [pF]	C_{ps2} [pF]	R_{load} [Ω]
First Prototype	1.8	44	44	14.2	14.2	42
Second Prototype	0.88	62.9	62.9	9.58	9.58	46.6

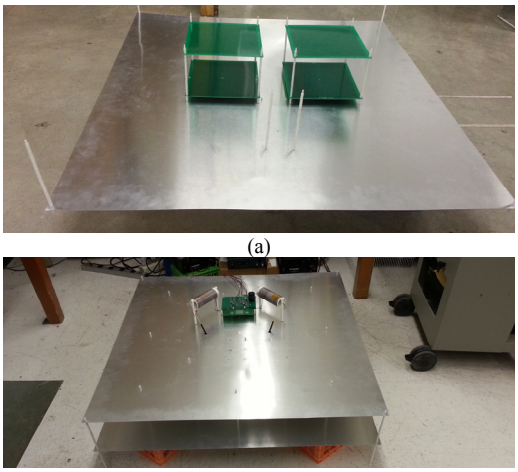

(a) (b)

Fig. 7. Photograph of the first prototype capacitive WPT system showing: (a) 17.68 cm × 17.68 cm coupling plates, and (b) complete system with metal sheets mimicking the vehicle chassis and road.

two large metal sheets in Fig. 7(b) are aluminum sheets that mimic the vehicle chassis and the road. The inductance and capacitance values used in the matching networks of the first prototype system are shown in Table I. The matching network capacitances are fully realized using the parasitic plate-to-road and plate-to-chassis capacitances. The required values for these capacitances are obtained by adjusting the distance between the coupling plates and the aluminum sheets shown in Fig. 7. The matching network inductors are implemented as single-layer air-core solenoids with quality factors greater than 250, and self-resonant frequencies greater than 20 MHz. Enhancement-mode GaN FETs (GaN Systems GS66504B) are used to implement the full- bridge inverter, which operates at a switching frequency of 6.78 MHz. Figure 8 shows the measured waveforms of the prototype capacitive WPT system delivering 193 W of output power. It is apparent from Fig. 8(a) that the minimum inductive loading required for ZVS of the inverter transistors is achieved. The prototype system achieves an efficiency of 90% and a power transfer density of 3 kW/m^2. This high performance is

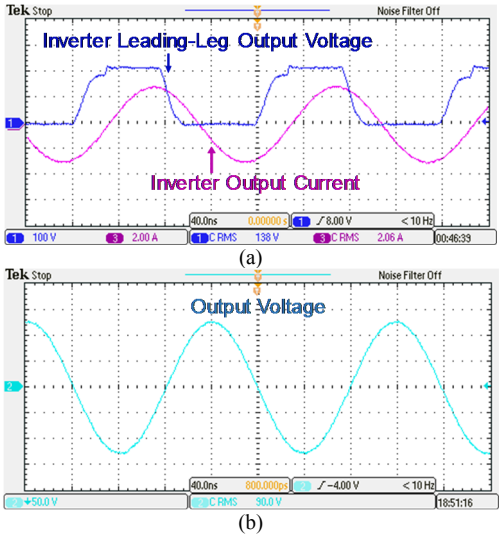

(a) (b)

Fig. 8. Measured waveforms for the prototype capacitive WPT system: (a) inverter output voltage and current, and (b) voltage across the load resistor.

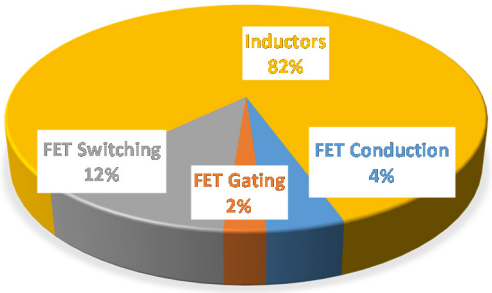

Fig. 9. Estimated loss breakdown of the first prototype capacitive WPT system when operating at 193 W of power transfer.

majorly attributable to the design procedure described earlier, and to a careful implementation of the air-core inductors to ensure that the designed quality factors and self-resonant frequencies are achieved in practice. An estimated loss breakdown of this prototype capacitive WPT system when operating at an output power of 193 W is shown in Fig. 9. It can be seen that the inductors account for the majority of the power losses in this system.

The second prototype capacitive WPT system is designed for higher power and higher power transfer density operation. To achieve higher power transfer density, the coupling plates in the second prototype are designed to be 52% smaller than the first prototype, with dimensions of 12.25 cm × 12.25 cm, resulting in a total coupling plate area of 300 cm^2, and an effective coupling capacitance C_{plate} of 0.88 pF. To be able to transfer higher power levels, this prototype utilizes higher current rated GaN FETs (GaN Systems GS66506T). These FETs have a larger output capacitance than those used in the first prototype. The matching network design for the second prototype is appropriately modified to account for the smaller plate size and larger output capacitance, and the resultant inductance and capacitance values are listed in Table I. The matching network capacitances in this system are also fully realized using the parasitic capacitances, and the matching network inductors are again implemented as single-layer air-core solenoids with quality factors greater than 250 and self-resonant frequencies greater than 20 MHz. A photograph of the second prototype capacitive WPT system is shown in Fig. 10. It can be seen that the coupling plates in this system are implemented using bare copper sheets, eliminating the losses and dielectric breakdown risk associated with the FR4 used in the PCB coupling plates of the first prototype. Figure 11 shows the measured waveforms of the second capacitive WPT system delivering 557 W of output power. It is apparent from Fig. 11(a) that this system also achieves ZVS of the inverter transistors. An estimated loss

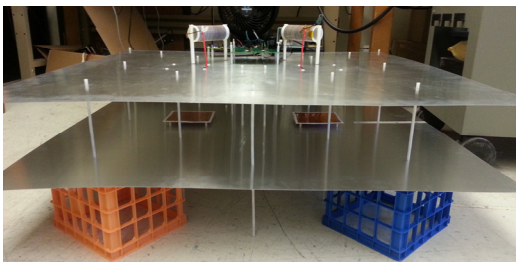

Fig. 10. Photograph of the second prototype capacitive WPT system with 12.25 × 12.25 cm coupling plates and metal sheets mimicking the vehicle chassis and the road.

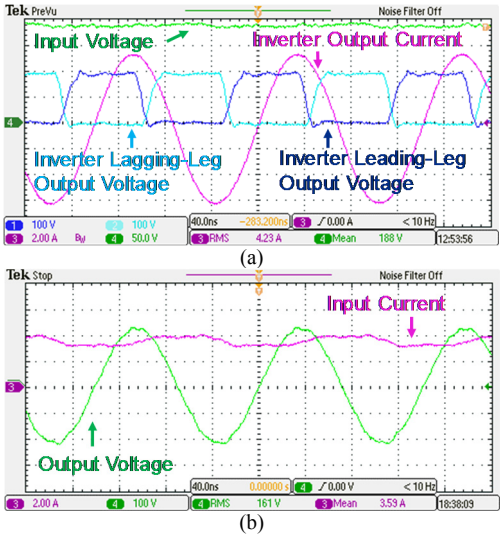

Fig. 11. Measured waveforms for the second prototype capacitive WPT system: (a) dc input voltage, inverter output voltage and current, and (b) voltage across the load resistor and dc input current.

breakdown of this prototype system when operating at 557 W of power transfer is presented Fig. 12, indicating again that the matching network inductors are the major loss contributors. This prototype capacitive WPT system achieves an efficiency of 82%, and a power transfer density of 18.5 kW/m^2, which is more than four times higher than the state-of-the-art of capacitive WPT systems.

V. Conclusions

This paper presents a high-performance large-air-gap capacitive WPT system for electric vehicle charging applications. This capacitive WPT system closely emulates a real-world vehicle charging scenario, implementing the capacitive coupler using two pairs of metal plates separated by a large air-gap, with two additional metal sheets mimicking the vehicle chassis and the road. This system achieves high efficiency by utilizing appropriately designed matching networks for gain and reactive compensation. The efficiency and reliability of the system are enhanced by utilizing the parasitic capacitances formed between the coupling plates and the chassis and road as the matching network capacitors; eliminating the need for high-voltage on-board capacitors. Two prototype 12-cm air-gap capacitive WPT systems operating at the ISM band frequency of 6.78 MHz have been designed, built and tested. The first prototype system transfers up to 193 W of power at greater than 90% peak efficiency, achieving a power transfer density of 3 kW/m^2. The second prototype system transfers up to 557 W of power at an efficiency of 82%, achieving a power transfer density of 18.5 kW/m^2, which exceeds the state-of-the-art of capacitive WPT systems by a factor of greater than four. These systems are suitable as single modules of a kilowatt-scale multi-modular capacitive WPT system.

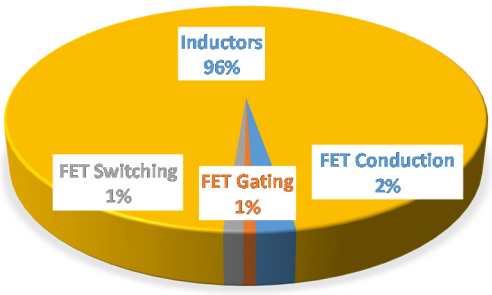

Fig. 12. Estimated loss breakdown of the second prototype capacitive WPT system when operating at 557 W of power transfer.

References

[1] G.A. Covic and J.T. Boys, "Modern Trends in Inductive Power Transfer for Transportation Applications," *IEEE Journal of Emerging and Selected Topics in Power Electronics*, vol. 1, no. 1, pp. 28-41, March 2013.

[2] A. Kumar, S. Pervaiz, Chieh-Kai Chang, S. Korhummel, Z. Popovic and K. K. Afridi, "Investigation of Power Transfer Density Enhancement in Large Air-Gap Capacitive Wireless Power Transfer Systems," *Proceedings of the IEEE Wireless Power Transfer Conference (WPTC)*, Boulder, CO, May 2015.

[3] F. Lu, H. Zhang, H. Hofmann and C. Mi, "A Double-Sided LCLC-Compensated Capacitive Power Transfer System for Electric Vehicle Charging," *IEEE Transactions on Power Electronics*, vol. 30, no. 11, pp. 6011-6014, November 2015.

[4] F. Lu, H. Zhang, H. Hofmann and C. Mi, "A CLLC-Compensated High Power and Large Air-Gap Capacitive Power Transfer System for Electric Vehicle Charging Applications," *Proceedings of the IEEE Applied Power Electronics Conference and Exposition (APEC)*, Long Beach, CA, March 2016.

[5] I. Ramos, K. Afridi, J. A. Estrada and Z. Popović, "Near-Field Capacitive Wireless Power Transfer Array with External Field Cancellation," *Proceedings of the IEEE Wireless Power Transfer Conference (WPTC)*, Aveiro, Portugal, May 2016.

[6] S. Sinha, A. Kumar, S. Pervaiz, B. Regensburger and K. K. Afridi, "Design of Efficient Matching Networks for Capacitive Wireless Power Transfer Systems," *Proceedings of the IEEE Workshop on Control and Modeling for Power Electronics (COMPEL)*, Trondheim, Norway, June 2016.

[7] H. Zhang, F. Lu, H. Hofmann and C. Mi, "A Loosely Coupled Capacitive Power Transfer System with LC Compensation Circuit Topology," *Proceedings of the IEEE Energy Conversion Congress and Exposition (ECCE)*, Milwaukee, WI, September 2016.

[8] K. Doubleday, A. Kumar, S. Sinha, B. Regensburger, S. Pervaiz and K. Afridi, "Design Tradeoffs in a Multi-Modular Capacitive Wireless Power Transfer System," *Proceedings of the IEEE PELS Workshop on Emerging Technologies: Wireless Power Transfer (WoW)*, Knoxville, TN, October 2016.

[9] F. Lu, H. Zhang, H. Hofmann, Y. Mei and C. Mi, "A Dynamic Capacitive Power Transfer System with Reduced Power Pulsation," *Proceedings of the IEEE PELS Workshop on Emerging Technologies: Wireless Power Transfer (WoW)*, Knoxville, TN, October 2016.

[10] F. Lu, H. Zhang, H. Hofmann, and C. Mi, "An Inductive and Capacitive Combined Wireless Power Transfer System with LC-Compensated Topology," *IEEE Transactions on Power Electronics*, vol. 31, no. 12, pp. 8471-8482, December 2016.

[11] H. Zhang, F. Lu, H. Hofmann, W. Liu and C. C. Mi, "A Four-Plate Compact Capacitive Coupler Design and LCL-Compensated Topology for Capacitive Power Transfer in Electric Vehicle Charging Application," *IEEE Transactions on Power Electronics*, vol. 31, no. 12, pp. 8541-8551, December 2016.

[12] International Commission on Non-Ionizing Radiation Protection, "ICNIRP Guidelines for Limiting Exposure to Time-Varying Electric, Magnetic and Electromagnetic Fields (1 Hz to 100 kHz)," *Health Physics*, vol. 99, no. 6, pp. 818–836, December 2010.

[13] A. Kumar, S. Sinha, A. Sepahvand and K. Afridi, "Improved Design Optimization for High-Efficiency Matching Networks," *IEEE Transactions on Power Electronics*, February 2017, available online.